

Elastic and Viscoelastic Properties of Calcium Silicate Hydrate

Z.C. Grasley¹, C.A. Jones², X. Li¹, E.J. Garboczi³, and J.W. Bullard³

¹Zachry Department of Civil Engineering, Texas A&M University, College Station, TX USA

zgrasley@civil.tamu.edu, lyd19881102@gmail.com

²Sandia National Laboratories, Albuquerque, NM USA

cajone@sandia.gov

³Engineering Laboratory, National Institute of Standards and Technology, Gaithersburg, MD USA

edward.garboczi@nist.gov, jeffrey.bullard@nist.gov

ABSTRACT

In order to effectively predict the mechanical properties of concrete and other cementitious materials, it is useful to understand the properties and deformation mechanisms on the nanometric length scale. Through a combined analytical, experimental, and numerical approach, insight has been gained into the nanoscale mechanical properties of calcium silicate hydrate. Using an atomic force microscope, elastic and viscoelastic properties of calcium silicate hydrate were measured. In addition, a novel computational model was developed to predict the evolution of apparent viscoelastic properties of hydrating cement paste. The results of the experiments and modeling suggest that inherent viscoelastic deformation of calcium silicate hydrate is not necessarily the sole (or primary) source of viscoelastic deformation of cementitious materials. Time-dependent dissolution of load bearing phases is suggested as an additional, significant mechanism for the apparent viscoelasticity of cementitious materials.

Keywords: C-S-H; Viscoelastic; Computational; FEM

1. Introduction

In general, researchers have traditionally attributed the viscoelastic behavior of concrete to the inherent viscoelastic behavior of the calcium silicate hydrate (C-S-H) phase [1]. This understanding of concrete viscoelasticity has led to the development of constitutive models for concrete viscoelastic behavior such as the solidification theory [2, 3]. Other mechanisms for the time-dependent deformation of cementitious materials have been proposed, however, including poromechanical effects and dissolution of load bearing phases [4, 5]. Several papers have documented the existence of poromechanical contributions to time-dependent deformation of saturated cementitious materials (see e.g. [6-9]), and Grasley and Leung [10, 11] have optimized the poromechanical viscoelastic effects in cementitious materials to enhance mechanical damping properties of concrete under oscillatory loading. However, it is known that the poromechanical components to viscoelastic deformation of cementitious materials are only substantial when the material is fully saturated. Conversely, the dissolution of load bearing phases has not been systematically investigated as a mechanism for viscoelastic deformation of cementitious materials.

The objective of the research reported herein is to evaluate the contribution of inherent C-S-H viscoelastic deformation and load bearing phase dissolution on the overall viscoelastic behavior of cementitious materials. Experimental measurements of the creep of C-S-H were performed along with computational modeling that evaluated the influence of the dissolution of load bearing phases.

2. Experimental study

2.1. Preparation of the samples for indentation tests

The specimens used in this study were cast from an ASTM C150 Type I/II cement with a water-to-cement mass ratio (w/c) of 0.4. The cement and water were mixed according to ASTM C305-99 and the resultant paste was placed into acrylic tubes with a square cross-section and an inner dimension of 1 cm. On one end, an acrylic plate was affixed with a two-part epoxy. The length of the tubes was approximately 10 cm. The fresh paste-filled molds were vibrated and placed under vacuum to remove any entrapped air. The specimens were then sealed and placed into a 98 % relative humidity (RH) room at a temperature of 23 °C for 24 h. Once the initial curing had taken place, the specimens were carefully demolded and placed in saturated lime water (2 g $\text{Ca}(\text{OH})_2$ per 1000 g water) for approximately 90 d.

The cured mini-beams were sliced perpendicular to the long axis of the beam into 3 mm thick 1 cm x 1 cm plates using an Isomet^{*} precision wet saw. The slices were allowed to dry in the laboratory environment and were then each affixed with cyanoacrylate glue to circular steel discs measuring 15 mm in diameter. The exposed flat surface of the cement paste sample was polished using techniques similar to those presented in [12], with the addition of final polishing using diamond slurries in five steps with diamond particle sizes ranging from 6 μm to 0.25 μm . In these final steps, the diamond slurry was placed on a glass plate and the specimen was manually oscillated against the glass. After each diamond-slurry polishing step, the specimen was wiped dry with denatured alcohol to remove any residue from the slurry.

2.2. Testing procedures

Indentation creep tests were performed on the specimens described above using both a traditional nanoindenter and an atomic force microscope (AFM). In this study, a Hysitron Triboindenter model TI-900 was used for traditional creep nanoindentation tests, which were conducted at room temperature (23 °C) and 50 % RH. The indenter was fitted with a typical diamond Berkovich indenter tip. Full details of the nanoindentation experimental equipment and procedure have been published elsewhere [13].

The AFM-based indentation experiments in this study were performed using a Veeco Dimension Icon AFM. For the AFM based experiments reported herein, the indentation depth varied but was generally in the range of a few hundred nanometers. AFM indentation tests were also performed at room temperature and relative humidity.

Unfortunately, the particular AFM used in this research could not reliably maintain feedback control on the cantilever deflection (applied force) signal. This prohibited true “creep” (constant stress state) experiments from being performed. On the other hand, the experiment could not be performed as a true “relaxation” (constant strain state) test either owing to cantilever deflection as the method of load application in the AFM. Given these limitations, the experiment was performed by applying a specified actuator rigid displacement step and then maintaining this step for a specified period of time. Fortunately, the load loss measured dur-

* Certain commercial equipment and/or materials are identified in this report in order to adequately specify the experimental procedure. In no case does such identification imply recommendation or endorsement by the National Institute of Standards and Technology, nor does it imply that the equipment and/or materials used are necessarily the best available for the purpose.

ing the test was only about 1 % to 2 %, which was deemed small enough to merit approximating the test as a creep test.

In order to select locations on the specimen surface to indent with the AFM, the surface was first imaged using the AFM. The morphology in the 5 micrometer square topographical image indicated that the material comprising the region imaged was entirely amorphous, and was thus assumed to be entirely C-S-H. A total of 125 indentations were performed of which 7 were discarded due to jumps in the displacement data indicating that the indentation was occurring on the edge of a feature such that slippage occurred. The majority of the tests were done in 3 x 3 grids in randomly selected locations in the imaged region.

2.2. Experimental results

The average measured uniaxial viscoelastic compliances (J), normalized by the zero time value, of cement paste measured using both nanoindenter and AFM are shown in Fig. 1. The curves show the many data points, while error bars are only displayed for three data points for each curve to give an idea of the measurement uncertainty. Measurements with the nanoindenter yield a higher creep rate than measurements performed with an AFM. Since the peak stress magnitude in the AFM test is significantly higher than in the nanoindenter test, this result is even more striking. A possible explanation for the higher creep rate exhibited in the nanoindenter test is the presence of multiple creep processes, whereas only inherent viscoelasticity of the C-S-H phase is present in the AFM. The AFM probes a much smaller volume than the nanoindenter, and is thus more closely approaching an intrinsic measurement of C-S-H properties. The nanoindenter, on the other hand, very likely probes multiple phases (both hydrated and unhydrated) simultaneously [14, 15]. The suggestion of Fig. 1 is that, since creep rate is higher when a larger volume of material, much of it presumably not C-S-H, is interacted with, C-S-H viscoelasticity cannot be the sole mechanism behind bulk viscoelastic response of cementitious materials.

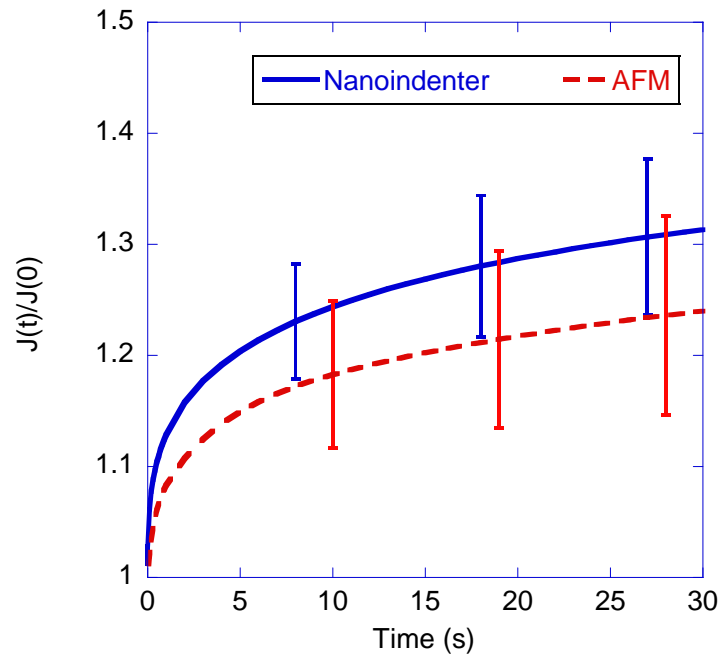


Fig. 1. Uniaxial viscoelastic compliance of C-S-H measured using a traditional nanoindenter and an AFM; values are normalized by instantaneous uniaxial compliance. Vertical bars indicate one standard deviation.

3. Computational modeling

3.1. Model development

Previous work on predicting constitutive properties of cement paste as a function of the evolving microstructure has included the prediction of the elastic moduli [16]. The prediction of the elastic moduli involved utilizing a microstructure model (CEMHYD3D [17]) to predict the evolution of the $100 \mu\text{m}^3$ microstructure resulting from hydration. At different ages, a 3D snapshot of the microstructure was taken from the model. Each voxel was assigned a particular phase, and the entire microstructure was meshed such that each voxel became one finite element. Elastic properties were assigned to each phase present based on literature values [16], and the resulting composite elastic properties were predicted through finite element analysis. The predicted properties agreed well with the measured elastic properties obtained from specimens fabricated using the same cement utilized as an input in the microstructure model.

The modeling undertaken in this work extends the previous prediction of elastic properties. First, a next-generation model for hydration called THAMES [18] is utilized to predict the evolution of the microstructure. Second, the finite element model is discretized in time in order to account for time and history dependent mechanical properties. Since the microstructure is evolving with time, it is important to have a snapshot of the microstructure at each time step in the finite element model. Furthermore, as hydration progresses, unhydrated phases that are transmitting stress are dissolved and replaced by other phases. A key assumption in the model is that if a certain voxel changes phase (e.g. from unhydrated C_3S to C-S-H), the stress transmitted through the original phase must be redistributed to surrounding phases and the new phase must form in a stress-free state in the deformed configuration. More specifically, at the first time step in the model a constant periodic strain boundary condition is applied to the microstructure. At the next time step, the microstructure for the age corresponding to the new time step is compared to the microstructure from the first time step. Any voxels that have changed phase are noted and are assumed to be infinitely compliant such that they cannot transmit stress. The new stress and strain fields (which yield a decrease in average composite stress in comparison to the previous time step) are then calculated for the microstructure based on this assumption and the same periodic strain boundary condition. The voxels for which phases changed are then replaced with the new phase and the model proceeds to the next time step.

As illustrated in Fig. 2, a redistribution of stress results in a time dependent elastic deformation (or stress relaxation) that could contribute to the apparent macroscopic viscoelasticity of cement paste. As it is easier to conceptually visualize, Fig. 2 describes how apparent viscoelastic deformation occurs under a constant applied macroscale stress. The new model discussed in this paper actually applies a constant periodic strain boundary condition, and thus models the stress relaxation process rather than creep. Considering either creep or relaxation, the effect of time-dependent dissolution of load-bearing phases is apparent viscoelasticity at the macroscale.

The computational model also allows one to incorporate intrinsic viscoelasticity of any given phase by defining a unique viscoelastic constitutive law for any given phase. Thus, one can model the viscoelasticity of cement paste where intrinsic creep (e.g. of C-S-H) and apparent creep (due to dissolution effects) are considered either individually or in tandem.

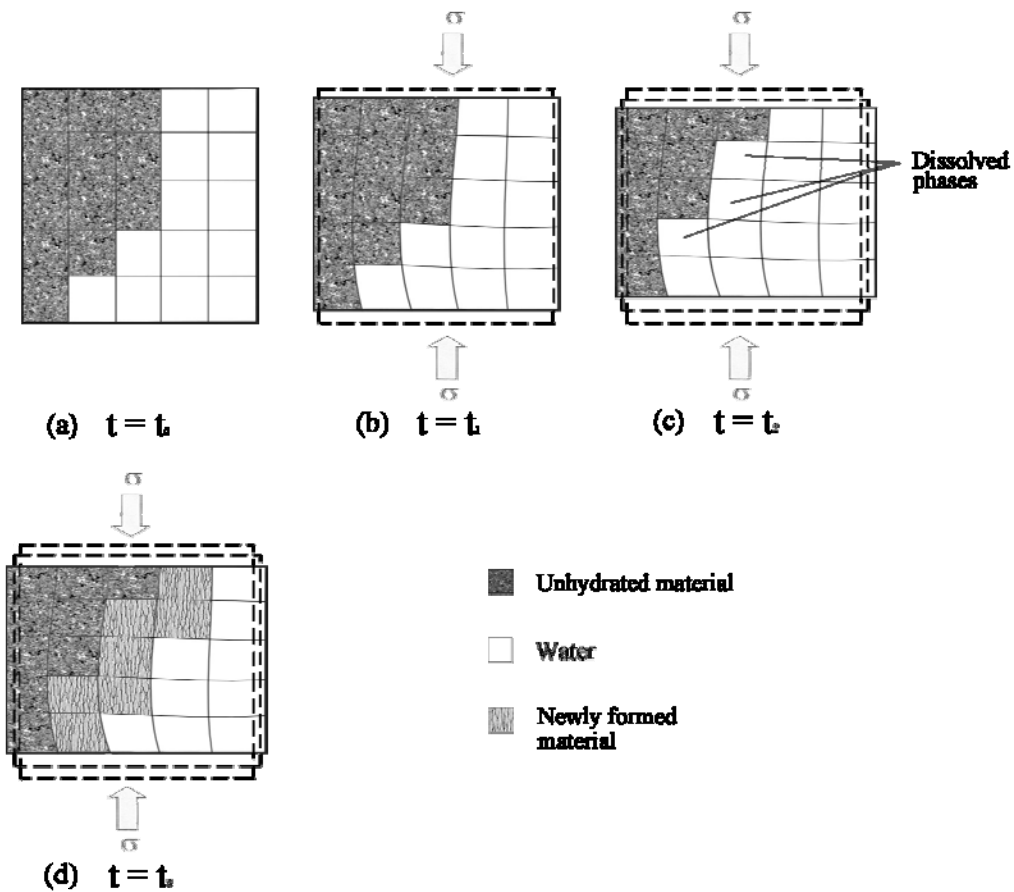


Fig. 2. Conceptual diagram of computational model simulating apparent viscoelastic behavior of hydrating cement paste where σ is a constant applied external macroscale stress and t is time elapsed. (a) Just before application of load a certain amount of load-bearing unhydrated material exists. (b) Just after the application of load, the body deforms elastically. (c) After some time under constant load, some load-bearing unhydrated material dissolves, increasing the stress on surrounding solid phases, which increases their elastic deformation (and thus the overall deformation of the composite microstructure). Because the elastic deformation due to phase dissolution does not occur instantly after application of the load, the result is an apparent viscoelastic deformation. (d) New phases form in the deformed configuration in a stress-free state.

3.2. Model simulations

To demonstrate the utility of the computational model, THAMES was utilized to predict the evolution of microstructure for 0.40 w/c and 0.45 w/c cement pastes for the same well-characterized cement used in Ref. [18]. The microstructures at different ages were then utilized in the finite element code to predict the evolution of apparent macroscopic viscoelastic Young's modulus. Fig. 3 shows the apparent viscoelastic Young's modulus of the 0.40 w/c paste with constant periodic strain boundary conditions applied at ages of 1 d and 7 d. In Fig. 3, the relaxation is due entirely to dissolution effects; that is, the phases were all considered to be elastic (no inherent viscoelasticity) using elastic properties taken from [16]. One can see in the figure that the apparent viscoelasticity due to dissolution effects is substantial. In fact, the magnitude of relaxation is such that dissolution effects should be considered in any mechanistic model of cement paste or concrete viscoelasticity. Additionally, one can see that since the rate of dissolution of phases slows as specimens age (since hydration rate slows with age)

the well-known aging effect of viscoelasticity reported in the literature [1] is also consistent with this dissolution mechanism.

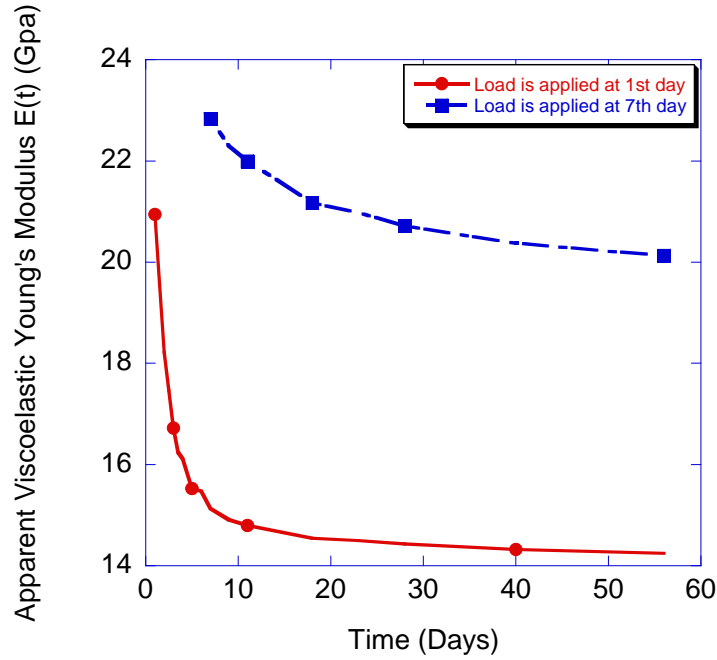


Fig. 3. Model behavior of apparent viscoelastic Young's modulus of 0.40 w/c cement paste when constant periodic strain boundary conditions are applied at either 1 d age or 7 d age. In this graph, viscoelasticity is considered to occur strictly due to dissolution of load bearing phases. The dissolution effect results in significant relaxation and is able to explain the aging effect of viscoelasticity.

While Fig. 3 demonstrates that dissolution effects are consistent with the apparent viscoelastic behavior seen in cementitious materials, the relative importance of dissolution effects in comparison to other potential mechanisms is not elucidated. Historically, the inherent viscoelasticity of C-S-H has been considered a primary mechanism of viscoelasticity of cementitious materials. In order to investigate whether or not either dissolution effects or inherent viscoelasticity of C-S-H should be considered primary viscoelastic deformation mechanisms of cementitious materials, a simulation was performed where dissolution effects were ignored and the relaxation was entirely attributable to inherent C-S-H viscoelasticity. Since the indentation experiments yielding the results reported in Fig. 1 last only 30 s (due to experimental challenges), they do not provide sufficient data for modeling creep or relaxation over several days. Therefore, for simulation purposes, the viscoelastic Young's modulus of C-S-H was assumed to be:

$$E(t) = 11.2 + 11.2 \exp(-t/\tau) \text{ GPa} \quad (1)$$

(where t is in units of d). This functional form was chosen so that $E(0)$ would be approximately correct [16] and such that only 50 % of this original value would be relaxed at $t \rightarrow \infty$. The relaxation time was set at $\tau = 5$ d to give a reasonable time scale in accord with many experiments [1].

The Poisson's ratio of the C-S-H was assumed to be time-independent and equal to 0.2. The elastic properties of all other phases in the microstructure were taken from [16]. Fig. 4 shows the results of the simulation. The viscoelastic Young's modulus of the 1 d old material was

generated by utilizing the 1 d old microstructure, which did not change as the simulated time changed. So the 1 d curve in Fig. 4 is how the Young's modulus would change with time for a 1 d old microstructure if only the C-S-H Young's modulus is considered to be viscoelastic. Likewise, the 28 d old viscoelastic Young's modulus was generated by utilizing the 28 d old microstructure (which was not allowed to evolve after the application of the constant periodic strain boundary conditions). Therefore, all of the time-dependent relaxation indicated in Fig. 4 is caused by relaxation of the inherently viscoelastic C-S-H phase.

Based on Fig. 4, one would conclude that a 28 d old cement paste would exhibit more relaxation than a 1 d old paste. This is in direct contrast to myriad experimental evidence of the aging viscoelastic properties of cement paste, where the older materials exhibit less relaxation (or creep) than the younger materials [1]. The reason that the results in Fig. 4 indicate higher relaxation for older materials is that the fraction of stress transmitted by C-S-H increases with age (since more C-S-H is present at later ages). Therefore, if C-S-H is the only viscoelastic phase in cement paste, more C-S-H results in more relaxation or creep. It appears that the inherent viscoelasticity of C-S-H is not likely the primary mechanism of cement paste viscoelasticity since this would yield behavior that would conflict with established experimental evidence of reduction in viscoelastic relaxation with age. The only way that C-S-H viscoelastic deformation could be the dominant mechanism in cement paste viscoelasticity would be if the dominant aging mechanism were inherent aging of the C-S-H rather than the hydration process. That is, the viscoelastic properties of C-S-H would need to dramatically evolve with the age of each C-S-H particle. While inherent aging of C-S-H has been suggested as a potential aging mechanism for cement paste [19, 20], it has been generally accepted that at early ages the hydration process is the dominant source of aging.

In light of the preceding arguments and simulation results, one can assert that inherent C-S-H viscoelasticity is probably not the primary mechanism of cement paste viscoelastic deformation, and inherent aging of C-S-H could be the dominant early age mechanism of cement paste aging. While long-term creep or relaxation indentation measurements of C-S-H have not yet been performed, this finding indicates that the results are likely to demonstrate that C-S-H creep is insufficient for fully predicting cement paste creep.

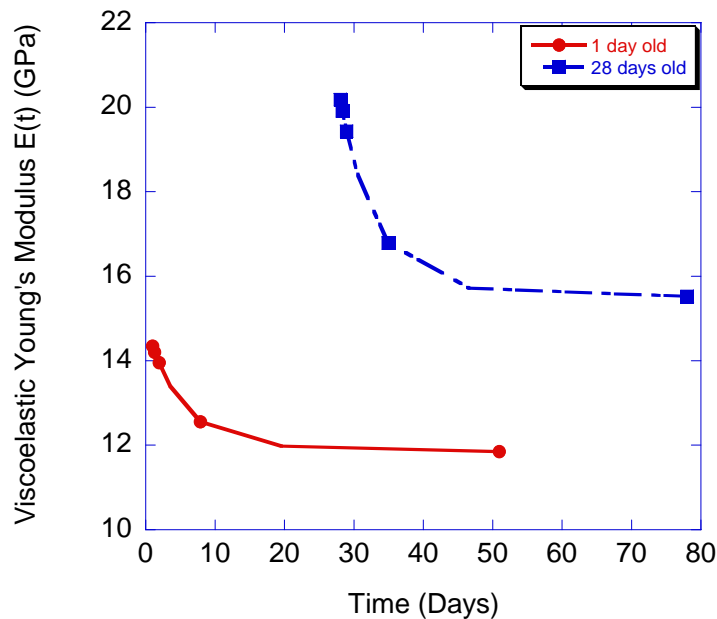


Fig. 4. Model predicted viscoelastic Young's modulus of 0.45 w/c cement paste displaced at ages of 1 d and 28 d. In this graph, all viscoelasticity is attributable to intrinsic viscoelasticity of C-S-H.

4. Discussion

Both the experimental and computational model results discussed in this paper indicate the need to consider additional mechanisms for cement paste viscoelasticity beyond inherent C-S-H viscoelasticity. The computational results suggest that dissolution of load bearing phases contributes significantly to the apparent viscoelasticity of cementitious materials. The dissolution effect is also able to adequately account for the aging effect of viscoelasticity noted in countless experiments. However, it is well-known that hydration slows dramatically after an age of about 28 d (under typical curing conditions) but creep continues long after 28 d. Therefore, one must consider mechanisms of viscoelasticity other than dissolution of unhydrated cement grains. One possibility that has not been fully explored is load-induced dissolution of hydration products; such a mechanism could explain how viscoelastic effects continue to occur once hydration has virtually ceased. As stress and strain states evolve within a loaded microstructure, the stress power (i.e. the product of the local velocity gradient and the local Cauchy stress) in each phase also evolves. Such an evolution might upset the local thermodynamic equilibrium such that solid phases that were stable under one local stress state might not be stable under another, resulting in their dissolution.

5. Conclusions

Nanoindentation creep experiments were performed using both a traditional nanoindenter and an AFM. The results indicate that creep of C-S-H on the nanometer length scale is less than what is observed on the micrometer length scale, indicating that an additional creep mechanism is present beyond intrinsic C-S-H creep. A computational model was developed to predict the viscoelastic properties of cement paste as a function of the evolving microstructure. The results from the computational model suggest that dissolution of load-bearing phases provides substantial apparent viscoelastic effects to cement paste. Furthermore, the model simulations suggest that intrinsic C-S-H viscoelasticity may not be the primary mechanism of cement paste viscoelasticity.

Future work is needed to clarify the relative importance of various mechanisms of cement paste viscoelasticity. In particular, dissolution of phases due to evolving stress power in the microstructure could potentially explain long-term viscoelastic effects, but needs to be experimentally or theoretically verified.

Acknowledgments

This research was supported in part by the National Science Foundation CAREER Award Program under grant number CMMI-0843979. Any opinions, findings, and conclusions or recommendations expressed in this material are those of the author(s) and do not necessarily reflect the views of the National Science Foundation. We would also like to acknowledge support from the NIST Engineering Laboratory Exploratory Research and Sustainable, High Performance Infrastructure Materials programs.

References

1. Mindess S, Young JF Darwin D. Concrete, 2nd ed. Upper Saddle River, NJ: Prentice Hall, Inc.; 2002.
2. Bažant Z. Viscoelasticity of solidifying porous material - concrete. *J Eng Mech* 1977; 103(EM6): 1049-1067.
3. Carol I Bažant ZP. Viscoelasticity with aging caused by solidification of nonaging constituent. *J Eng Mech* 1993; 119(11): 2252-2259.
4. Jensen OM Hansen PF. Autogenous deformation and change of the relative humidity in silica fume-modified cement paste. *ACI Mater J* 1996; 93(6): 539-543.
5. Suter M Benipal G. Constitutive model for aging thermoviscoelasticity of reacting concrete I: Theoretical formulation. *Mech Time Depend Mater* 2010; 14(3): 277-290.
6. Coussy O Monteiro PJM. Poroelastic model for concrete exposed to freezing temperatures. *Cem Concr Res* 2008; 38(1): 40-48.
7. Grasley Z, Scherer G, Lange D Valenza J. Dynamic pressurization method for measuring permeability and modulus: II. Cementitious materials. *Mater Struct* 2007; 40(7): 711-721.
8. Ulm FJ, Constantinides G Heukamp FH. Is concrete a poromechanics material? A multiscale investigation of poroelastic properties. *Mater Struct* 2004; 37(265): 43-58.
9. Vichit-Vadakan W Scherer GW. Measuring permeability of rigid materials by a beam-bending method: Iii, cement paste. *J Am Ceram Soc* 2002; 85(6): 1537-1544.
10. Leung CK Grasley ZC. Poroelastic damping of cementitious materials. *J Mater Civ Eng* 2011; doi:10.1061/(ASCE)MT.1943-5533.0000368:
11. Grasley ZC Leung C. Quasi-static axial damping of poroviscoelastic cylinders. *J Eng Mech* 2011; 137(8): 561-570.
12. Kjellsen KO, Monsøy A, Isachsen K Detwiler RJ. Preparation of flat-polished specimens for SEM-backscattered electron imaging and X-ray microanalysis—importance of epoxy impregnation. *Cem Concr Res* 2003; 33(4): 611-616.
13. Jones CA Grasley ZC. Short-term creep of cement paste during nanoindentation. *Cem Concr Comp* 2011; 33(1): 12-18.
14. Chen JJ, Sorelli L, Vandamme M, Ulm F-J Chanvillard G. A coupled nanoindentation/SEM-EDS study on low water/cement ratio portland cement paste: Evidence for C-S-H/Ca(OH)₂ nanocomposites. *J Am Ceram Soc* 2010; 93(5): 1484-1493.
15. Trtik P, Munch B Lura P. A critical examination of statistical nanoindentation on model materials and hardened cement pastes based on virtual experiments. *Cem Concr Comp* 2009; 31(10): 705-714.
16. Haecker CJ, Garboczi EJ, Bullard JW, Bohn RB, Sun Z, Shah SP, et al. Modeling the linear elastic properties of portland cement paste. *Cem Concr Res* 2005; 35(10): 1948-1960.

17. Bentz DP. Quantitative comparison of real and CEMHYD3D model microstructures using correlation functions. *Cem Concr Res* 2006; 36(2): 259-63.
18. Bullard JW, Lothenbach B, Stutzman PE Snyder KA. Coupling thermodynamics and digital image models to simulate hydration and microstructure development of portland cement pastes. *J Mater Res* 2011; 26(4): 609-622.
19. Thomas JJ Jennings HM. A colloidal interpretation of chemical aging of the C-S-H gel and its effects on the properties of cement paste. *Cem Concr Res* 2006; 36(1): 30-38.
20. Bentur A, Milestone NB Young JF. Creep and drying shrinkage of calcium silicate pastes. II: Induced microstructural and chemical changes. *Cem Concr Res* 1978; 8: 721-732.